AD-A192 469 EXCITED-STATE ENERGETICS AND DYNAMICS OF LARGE MOLECULES COMPLEXES AND CLUSTERS(U) TEL-AVIV UNIV (ISRAEL) DEPT OF CHEMISTRY J JORTNER ET AL MAR 86 1/1

UNCLASSIFIED DAJA45-85-C-0008 F/G 21/2 NL

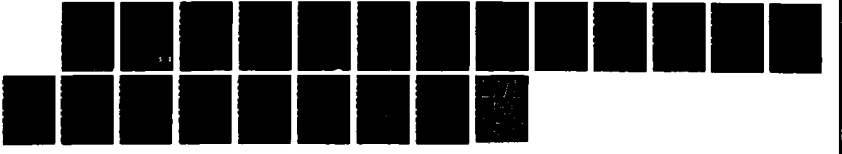

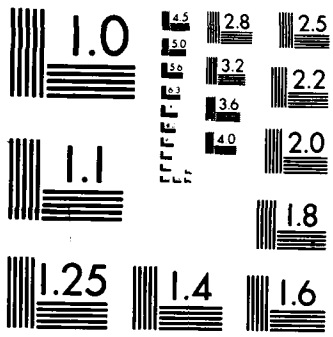
1.0
1.1
1.25
1.4
1.6
1.8
2.0
2.2
2.5
2.8
3.2
3.6
4.0
4.5
5.0
5.6

4759-CH-01

DTIC FILE COPY

(2)

AD-A192 469

PROGRESS REPORT FOR THE PERIOD OCTOBER, 1985-MARCH, 1986

3rd Periodic Report

1. Title: EXCITED-STATE ENERGETICS AND DYNAMICS OF LARGE MOLECULES, COMPLEXES AND CLUSTERS

2. Principal Investigator: Professor Joshua Jortner

3. Associate Investigator: Professor Uzi Even

4. Contractor: School of Chemistry
Tel Aviv University
Tel Aviv 69978
Israel

5. Contract No: DAJA45-85-C-0008

The Research reported in this document has been made possible through the support and sponsorship of the U.S. Government through its European Research Office of the U.S. Army. This report is intended only for the internal management use of the Contractor and the U.S. Government.

DTIC
ELECTE
MAR 3 0 1988
S D
E

This document has been approved for public release and sale; its distribution is unlimited.

88 3 23 120

6. PROGRESS IN TECHNICAL APPROACH

New techniques for spectroscopy in supersonic expansions and in the development of specific supersonic sources were developed.

6.A Vacuum Ultraviolet Absorption Spectroscopy in Supersonic Expansions. We have combined the techniques of vacuum ultraviolet (VUV) spectroscopy together with planar supersonic jets, which allows for the interrogation of absorption spectra of large molecules cooled in supersonic expansions in the near VUV region. The experimental setup consists of a high pressure Xe lamp, CaF_2 optics, a vacuum ultraviolet spectrograph and a nozzle slit (0.27x90 mm, repetition rate 9 Hz and gas pulse duration 300 μsec). The characteristics of this spectroscopic setup are: (i) Energy range 6-10 eV. (ii) Spectral resolution 0.1 Å. (iii) Routine measurements of high-energy absorption spectra. (iv) Interrogation of fluorescence excitation spectra of the parent molecule or its photoproducts with limiting quantum yields of $Y \geq 10^{-4}$.

6.B Development of Conical Nozzles for Supersonic Jets. Conical nozzles (nozzle opening angle $\theta = 30°$, and nozzle diameter D = 0.3 mm) were constructed and used in conjunction with a magnetic pulsed valve. The use of conical nozzles considerably enhances clustering in supersonic expansions, facilitating studies of large van der Waals complexes and clusters.

7. ACCOMPLISHMENTS OF OBJECTIVES

7.A Energetics of Rydberg States of Jet Cooled Molecules. VUV absorption spectra of benzene, benzene-D_6 and naphthalene cooled in planar supersonic expansions were measured over the range 2000-1600 Å, providing evidence on energetics, line broadening and interference effects.

Accession For
NTIS GRA&I ☒
DTIC TAB ☐
Unannounced ☐
Justification
By
Distribution/
Availability Codes
Dist | Avail and/or Special
A-1

7.B Rydberg States of Anthracene. Several Rydberg transitions of jet-cooled anthracene were observed in the spectral region 1900-2000 Å. These Rydbergs are superimposed on a broad "background" of $\pi\pi^*$ transitions. Up to now no fluorescence from Rydberg states of polyatomic molecules has been reported. The 1997 Å n=3 Rydberg of anthracene reveals fluorescence with a quantum yield of $\sim$ 5%. This fluorescence originates from internal conversion R $\rightsquigarrow$ S_1 followed by $S_1 \longrightarrow S_0$ emission, as documented by the spectral distribution of the dispersed fluorescence.

7.C Intramolecular Relaxation of Rydberg States. Information on intramolecular dynamics of extravalence excitations of benzene was obtained from lineshape analysis. The lineshape of the $^3P_{xy}(0)$ Rydberg is Lorentzian, whose homogeneous width result in the lifetime τ = 0.19±0.02 psec for C_6H_6 and τ = 0.22±0.02 psec for C_6D_6. Semiquantitative information on the lifetimes of some Rydbergs of anthracene was obtained, which fall in the range of $\sim$ 0.1 psec. These lifetime data imply that (i) the relaxation of the Rydberg is characterized by moderate energy gap(s), and (ii) the electronic relaxation rate of the Rydberg is considerably less efficient than that of the intravalence excitation in the same energy domain.

7.D Interference Effects between Extravalence and Intravalence Molecular Excitations. We have searched for Rydberg-valence interference effects in large molecules, which are expected to be exhibited in asymmetric Fano-type lineshapes in absorption. For "isolated" Rydbergs, which are superimposed on a $\pi\pi^*$ transition in benzene, naphthalene and anthracene, the absorption lineshapes are symmetric Lorentzians. No line asymmetry and no antiresonances characteristic of Fano profiles were found in that case. The absence of interference effects in this case reveals the manifestation of random interstate coupling of R with the π^* manifold. The random coupling erodes all interference effects. The situation is different for nearly lying Rydbergs, where pronounced R-R-valence interference effects were observed in the absorption spectra of jet-cooled naphthalene in the spectral region 1600-1650 Å, providing information on the homogeneous contribution to high-energy molecular coupling phenomena.

7.E Rotational State Dependence of Intramolecular Dynamics. Rotational effects on interstate coupling are of considerable current interest. Absolute fluorescence quantum yields from photoselected rotational states were measured for the electronic origins of the S_1 state of pyrazine. Strong rotational state dependence was observed providing novel information on interstate coupling for the intermediate level structure. This unique information cannot be extracted from time-resolved decay lifetimes.

7.F The Coupling between Intrastate Vibrational Energy Redistribution and Interstate Electronic Relaxation. We have documented some universal characteristics of the decay lifetimes and fluorescence quantum yields from the S_1 manifold of large molecules, which originate from the coupling between intrastate vibrational energy redistribution and interstate electronic relaxation. The time-resolved total fluorescence decay excited by a psec laser from the S_1 state of jet-cooled 9CN-anthracene exhibits nonexponential decay in the energy range E_V = 1200-1740 cm^{-1} above the S_1 origin, which does not originate from dephasing but rather manifests the effects of intrastate intermediate level structure for vibrational energy redistribution on intersystem crossing.

7.G Fluorescence Quantum Yields for Highly-Excited States of Large Molecules. Fluorescence quantum yields Y from high electronic excitations of naphthalene, anthracene and tetracene in the energy range 5.0-6.5 eV have been recorded. Y exhibits an exponential dependence on the excess vibrational energy with the slope decreasing with increasing size of the molecule, i.e., the vibrational density of states. These data are characteristic of internal conversion from S_1 to S_0. These results are of interest regarding recent astrophysical implications of high-energy photophysics of large aromatic hydrocarbons in outer space.

7.H Photoisomerization Dynamics of Trans-Stilbene and of Cis-Stilbene. Time-resolved fluorescence lifetimes from photoselected states of trans-stilbene were recorded by the techniques of picosecond spectroscopy in jets using a mode-locked dye laser and a fast photon counting system. Decay lifetimes as short as 100±30 psec were recorded. Extensive information on the energy dependence of the

isomerization rates of alkyl stilbenes was obtained, providing information on the role of intramolecular vibrational distribution on the photochemistry in an isolated molecule. The absorption spectrum of jet-cooled cis-stilbene is broad and no vibrational structure could be resolved due to the congestion of broadened low-frequency vibrational excitation. From the low quantum yield $Y \lesssim 2 \times 10^{-4}$ we infer a S_1 lifetime of $\tau \lesssim 0.4$ psec, which indicates ultrafast relaxation of this molecule.

7.I Photoisomerization Dynamics of Alkyl Substituted Trans-Stilbene. A central issue pertaining to isolated-molecule photochemistry involves the role of intramolecular vibrational relaxation in determining intramolecular dynamics. We have attempted to increase the density of vibrational states by alkyl substitution of trans-stilbene and have explored the isomerization dynamics by picosecond time-resolved spectroscopy. We have obtained the counter-intuitive result that alkyl substitution of trans-stilbene enhances the photoisomerization rates, while general arguments based on the role of IVR and the implications of statistical theories indicate that the rate should be retarded. The results can be accounted for by the modification of the molecular parameters, i.e., threshold energy, by alkyl substitution.

7.J Energy-Resolved Photoisomerization Rates. The dynamics of the S_1 and S_2 electronically excited singlet states of diphenylbutadiene was interrogated by fluorescence quantum yield measurements over the very broad energy domain of 0-7500 cm^{-1} above the (false) S_1 origin. The issues of the lack of mode selectivity and the applicability of statistical theories for the description of isolated-molecule photochemistry were explored.

7.K van der Waals Complexes of Porphyrins. Excited-state energetics and dynamics of large complexes consisting of porphyrins bound to rare-gas atoms were explored. Detailed spectroscopic information on the $S_0 \rightarrow S_1$ and $S_0 \rightarrow S_2$ transitions of the free-base porphine·Ar complex was obtained, providing insight into the structure of this complex as well as resulting in a novel mechanism for microscopic solvent shifts induced by configurational distortions, which are due to complexing.

7.L Coupling between Intramolecular and Intermolecular Nuclear Motion in Complexes. Intermolecular vibrations of large van der Waals complexes, which involve the motion of the ligand relative to the large molecule, provide an analogue for surface vibrational motion in a finite system and constitute the precursors of phonon modes in condensed phases. Information on the coupling between intermolecular and intramolecular vibrational motion was obtained for the trans-stilbene·Ar complex.

7.M Electron Localization in Clusters. Small clusters exhibit unique physical and chemical phenomena, which are both of fundamental and technological significance, and provide ways and means to explore the "transition" from molecular to condensed-matter systems. We have provided a theoretical study of the structure, energetics and dynamics of an excess electron interacting with an alkali-halide cluster, which was explored by the quantum path integral molecular dynamics method. These studies establish various compositional, structural and size dependence of bulk and surface localization mechanisms of the dynamic process induced by electron attachment.

7.N Vibrational Predissociation Induced by Exciton Trapping in Rare-Gas Clusters. The dynamics of exciton trapping, vibrational energy transfer and vibrational predissociation in an electronically excited state of Ar_{13} clusters was explored by classical molecular dynamics. This study constitutes an application of this technique for the dynamics of electronically excited states of large systems. New mechanisms of ultrafast ($\sim$ 10 psec) vibrational energy flow induced by short-range repulsion were documented. In these systems vibrational energy redistribution does not occur and mode selective excitation prevails. In small (n=13) clusters the consequences of vibrational energy flow results in reactive vibrational predissociation, leading to the "evaporation" of Ar atoms for the cluster. In layer (n=55) clusters a transition from molecular-type reactive behavior to nonreactive vibrational relaxation, which is characteristic of condensed phases, was exhibited.

8. PUBLICATIONS

The following manuscripts, supported by this research grant, were prepared and submitted for publication:

(1) A. Amirav and J. Jortner
Vacuum Ultraviolet Absorption Spectroscopy in Supersonic Expansions
J. Chem. Phys. (Communication) 82, 4378 (1985)

(2) A. Amirav and J. Jortner
Rotational and Vibrational State Dependence on Intramolecular Coupling and Dynamics in the S_1 State of Pyrazine
J. Chem. Phys. (in press)

(3) J. Troe, A. Amirav and J. Jortner
Energy-Resolved and Thermalized Photoisomerization Rates of Diphenyl-Butadiene
Chem. Phys. Letters 115, 245 (1985)

(4) A. Amirav, M. Sonnenschein and J. Jortner
Interstate Coupling and Dynamics of Excited Singlet States of Isolated Diphenylbutadiene
Chem. Phys. 102, 305 (1986)

(5) U. Even, Z. Berkovitch-Yellin and J. Jortner
Electronic Excitations of the Free-Base Porphine·Ar van der Waals Complex
Canad. J. Chem. (C. Sandorfy-Special Issue) 63, 2073 (1985)

(6) D. Bahatt, U. Even and J. Jortner
Coupling between Intramolecular and Intermolecular Nuclear Motion in a Large van der Waals Complex
Chem. Phys. Letters 117, 527 (1985)

8. PUBLICATIONS (cont'd)

(7) Klaus Rademann, Uzi Even, Shlomo Rozen and J. Jortner
Photoisomerization Dynamics of Alkyl Substituted Stilbenes in Supersonic Jets.
Chem. Phys. Lett. (in press)

(8) A. Amirav, J. Jortner, S. Okajima and E. C. Lim
Manifestations of Intramolecular Vibrational Energy Redistribution on Electronic Relaxation in Large Molecules
Chem. Phys. Letters (in press)

(9) U. Landman, D. Scharf and J. Jortner
Electron Localization in Alkali-Halide Clusters
Phys. Rev. Letters 54, 1860 (1985)

(10) Dafna Scharf, Uzi Landman and Joshua Jortner
Energetics and Dynamics of Clusters
Proc. of the Int'l School of Physics "Enrico Fermi", Italy, July, 1985 (in press)

(11) D. Scharf, U. Landman and J. Jortner
Vibrational Predissociation Induced by Exciton Trapping in Inert-Gas Clusters
Chem. Phys. Letters (in press)

Vacuum ultraviolet absorption spectroscopy in supersonic expansions

Aviv Amirav and Joshua Jortner
Department of Chemistry, Tel Aviv University, 69978 Tel Aviv, Israel

(Received 18 December 1984; accepted 1 March 1985)

Remarkable progess has been accomplished in the area of molecular spectroscopy in supersonic expansions, which unveiled many facets of excited-state energetics and dynamics of large molecules excited in the energy range 0.2–6 eV.[1–4] Photoselective molecular excitation in jets above 6 eV is expected to open new horizons in the areas of extravalence spectroscopy, nonreactive and reactive intramolecular dynamics, and state selective molecular photochemistry.[5] A significant step in this direction was undertaken recently by three- and four-photon ionization studies[6–9] in jets and by femtosecond time-resolved investigations[10] of Rydberg states. We wish to report on the merger between the techniques of vacuum ultraviolet (VUV) spectroscopy and supersonic jets, which allows for the interrogation of absorption spectra of large molecules in supersonic expansions in the near VUV (6–9 eV) region. The techniques of absorption spectroscopy in seeded, planar, pulsed, supersonic expansions[11–13] were adopted for VUV absorption studies. Planar supersonic jets of Ar seeded with benzene, benzene-D_6 or naphthalene were expanded from a nozzle slit (dimensions 0.27×90 mm, repetition rate 9 Hz and gas pulse duration 300 μs) and the characteristic rotational temperatures were $T_R \simeq 20$ K. Light (spectral range 1500–2000 Å) from a modified short-arc high-pressure Xe lamp (EG & G Model FX 193U), which was fitted with a sapphire or CaF_2 window, was focused with an $f = 4$ CaF_2 lens onto the jet parallel to the nozzle slit at a distance $x = 8$ mm. The light beam was split by a CaF_2 plate and monitored by two photomultipliers coated with a (tetraphenyl butadiene) convector, both before and after crossing the planar jet. The absorption $\Delta I/I_0$ was normalized to the incident light intensity.

VUV absorption spectra of jet-cooled aromatic molecules provided information on intramolecular dynamics of odd-parity Rydberg states and an interference between Rydberg and intravalence excitations. The electronic origin of the $3P_{x,y}(^1A_{2u})$ Rydberg excitation [$3P_{x,y}(0)$] of benzene and of benzene-D_6 (Fig. 1) is superimposed on the $^1A_{1g} \rightarrow {}^1E_{1u}$ intravalence transition.[14,15] The energy of $3P_{x,y}(0)$ (55 877 cm^{-1} for C_6H_6 and 55 946 cm^{-1} for C_6D_6) is in accord with one-[14,15] and three-photon[16] bulb spectroscopy. The line shape of $3P_{x,y}(0)$ is a Lorentzian (Fig. 1) with a width (FWHM) of $\Delta = 32.7 \pm 3.1$ cm^{-1} for C_6H_6 and $\Delta = 29.0 \pm 2.0$ cm^{-1} for C_6D_6. The homogeneous linewidths Γ and lifetimes τ obtained after correction for instrumental resolution are $\Gamma = 28 \pm 3$ cm^{-1} ($\tau = 0.19 \pm 0.02$ ps) for C_6H_6, and $\Gamma = 24 \pm 2$ cm^{-1} ($\tau = 0.22 \pm 0.02$ps) for C_6D_6. Our value *pf* Γ for $3P_{x,y}(0)$ is close to the linewidths of 27–33 cm^{-1} reported[6] for the vibronically induced two-photon transitions of this Rydberg transition. A small ($\sim 10\%$) normal deuterium isotope effect on the relaxation rate may exist, which is, however, within our experimental uncertainty, implying that the electronic relaxation process of $3P_{x,y}(0)$ is characterized by moderate energy gap(s). The homogeneous line broadening of the $^1A_{1g} \rightarrow {}^1E_{1u}$ intravalence excitation of jet-cooled benzene exceeds Γ for $3P_{x,y}(0)$ by about one to two orders of magnitude, which is in accord with old arguments,[17] so that the intramolecular relaxation of the intravalence $^1E_{1u}$ excitation presumably occurs within ~ 10 fs, i.e., on a time scale comparable with a vibrational period. The Lorentzian line shape of $^1A_{1g} \rightarrow 3P_{x,y}(0)$ provides compelling evidence for the absence of Rydberg-intravalence interference effects[15,18,19] in benzene, which is in accord with Rice *et al.*[15] The absence of Fano interference effects[20] can be rationalized within the framework of a random coupling model[21,22] for the $3P_{x,y}(0)$–$^1E_{1u}$ interstate coupling terms and for the $^1A_{1g} \rightarrow {}^1E_{1u}$ transition moments to the homogeneously broadened background manifold, which erode all interference effects.[21,22] Pronounced Rydberg-intravalence interference effects[18] are exhibited in the spectrum of jet-cooled naphthalene (Fig. 2). The excessive line broadening of the resonance, e.g., $\Gamma = 80$ cm^{-1} ($\tau = 70$ fs) for the $R_c^5 + 1360$ transition (Fig. 2), is close to the corresponding

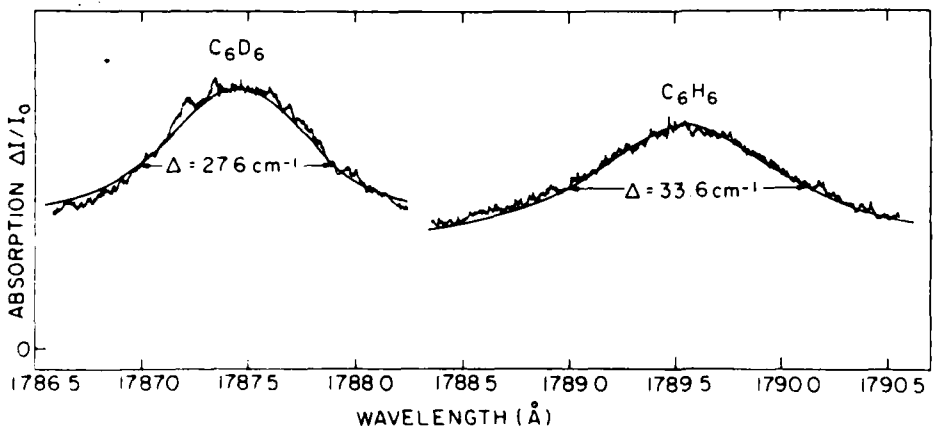

FIG. 1. Absorption spectra of the $^1A_{1g} \rightarrow 3P_{x,y}(A_{2u})$ electronic origin of benzene and benzene-D_6 in pulsed planar supersonic expansions of Ar at $p = 105$ Torr. The spectral resolution is 0.45 Å. The base line is marked as zero on the intensity scale. The solid curves represent fits of the line shape $L(\lambda)$ to a Lorentzian superimposed on a constant background $L(\lambda) = A + C/[(\lambda - \lambda_0)^2 + (\Delta/2)^2]$. For C_6H_6: $A = 5.7$, $C = 17.2$ (in arbitrary units), $\lambda_0 = 1789.65$ Å and $\Delta = 1.08$ Å (33.7 cm^{-1}) while for C_6D_6: $A = 6.5$, $C = 12.6$ (in arbitrary units), $\lambda_0 = 1787.45$ Å and $\Delta = 0.88$ Å (27.5 cm^{-1}).

 0021-9606/85/094378-02$02.10 © 1985 American Institute of Physics

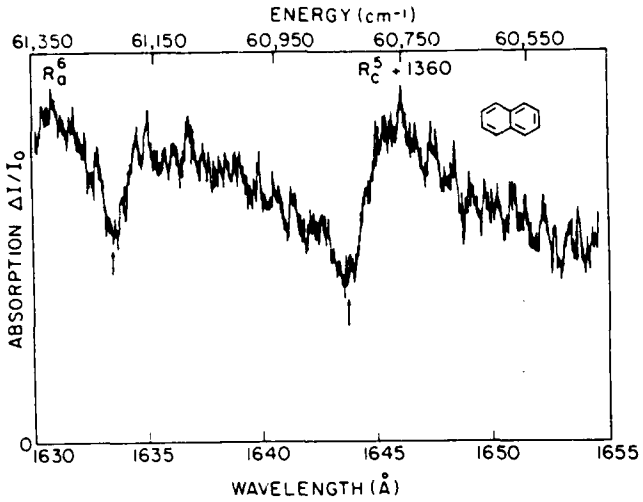

FIG. 2. The absorption spectra of naphthalene in pulsed planar expansions of Ar ($p = 105$ Torr) in the region 1630–1650 Å. The spectral resolution is 0.5 Å. The antiresonances corresponding to the $R_c^5 + 1360$ and to the R_a^6 Rydberg states (according to the assignment of Refs. 15 and 19) are marked by arrows.

room temperature value $\Gamma = 75\ \text{cm}^{-1}$,[15,19] whereupon the excessive homogeneous broadening make the thermal congestion effects. Our spectroscopic approach can readily be extended throughout the LiF region (up to 11 eV) and will contribute towards the elucidation of the microscopic aspects of intramolecular dynamics and photochemistry.

AA acknowledges the partial support of the work by the Basic Research Fund of the Israel Academy of Sciences, Jerusalem.

[1]D. H. Levy, Annu. Rev. Phys. Chem. **31**, 197 (1980).
[2]A. Amirav, U. Even, and J. Jortner, J. Chem. Phys. **74**, 3745 (1981).
[3]J. A. Syage, W. R. Lambert, P. M. Felker, A. H. Zewail, and R. M. Hochstrasser, Chem. Phys. Lett. **88**, 266 (1982).
[4]B. J. Van der Meer, H. Th. Jonkman, J. Kommandeur, and W. L. Meerts, Chem. Phys. Lett. **92**, 565 (1982).
[5]J. Jortner and S. Leach, J. Chim. Phys. **77**, 7 (1980).
[6]R. L. Whetten, K. J. Fu, and E. R. Grant, J. Chem. Phys. **79**, 2626 (1983).
[7]S. R. Grubb, R. L. Whetten, A. C. Albrecht, and E. R. Grant, Chem. Phys. Lett. **108**, 420 (1984).
[8]S. G. Grubb, C. E. Ottis, R. L. Whetten, E. R. Grant, and A. S. Albrecht, J. Chem. Phys. **82**, 1135 (1985).
[9]R. L. Whetten, K. J. Fu, and E. R. Grant, Chem. Phys. **90**, 155 (1984).
[10]J. M. Wiesenfeld and B. I. Greene, Phys. Rev. Lett. **51**, 1745 (1983).
[11]A. Amirav and J. Jortner, Journal **94**, 545 (1983).
[12]A. Amirav and J. Jortner, Journal **95**, 295 (1983).
[13]A. Amirav, M. Sonnenschein, and J. Jortner, Chem. Phys. Lett. **100**, 488 (1983).
[14]P. G. Wilkinson, Can. J. Phys. **34**, 596 (1956).
[15]R. Scheps, D. Florida, and S. A. Rice, J. Chem. Phys. **56**, 295 (1972).
[16]P. M. Johnson and G. M. Konenowski, Chem. Phys. Lett. **97**, 53 (1983).
[17]J. Jortner, J. Chim. Phys. **1970**, 10.
[18]J. Jortner, and G. C. Morris, J. Chem. Phys. **51**, 3689 (1969).
[19]D. Florida, R. Scheps, and S. A. Rice, Chem. Phys. Lett. **15**, 490 (1972).
[20]U. Fano, Phys. Rev. **124**, 1866 (1961).
[21]M. L. Sage and J. Jortner, Chem. Phys. Lett. **62**, 451 (1979).
[22]S. D. Druger, J. Chem. Phys. **67**, 3238, 3249 (1977).

Vacuum ultraviolet absorption spectroscopy in supersonic expansions

Aviv Amirav and Joshua Jortner
Department of Chemistry, Tel Aviv University, 69978 Tel Aviv, Israel

(Received 18 December 1984; accepted 1 March 1985)

Remarkable progess has been accomplished in the area of molecular spectroscopy in supersonic expansions, which unveiled many facets of excited-state energetics and dynamics of large molecules excited in the energy range 0.2–6 eV.[1–4] Photoselective molecular excitation in jets above 6 eV is expected to open new horizons in the areas of extravalence spectroscopy, nonreactive and reactive intramolecular dynamics, and state selective molecular photochemistry.[5] A significant step in this direction was undertaken recently by three- and four-photon ionization studies[6–9] in jets and by femtosecond time-resolved investigations[10] of Rydberg states. We wish to report on the merger between the techniques of vacuum ultraviolet (VUV) spectroscopy and supersonic jets, which allows for the interrogation of absorption spectra of large molecules in supersonic expansions in the near VUV (6–9 eV) region. The techniques of absorption spectroscopy in seeded, planar, pulsed, supersonic expansions[11–13] were adopted for VUV absorption studies. Planar supersonic jets of Ar seeded with benzene, benzene-D_6 or naphthalene were expanded from a nozzle slit (dimensions 0.27×90 mm, repetition rate 9 Hz and gas pulse duration 300 μs) and the characteristic rotational temperatures were $T_R \simeq 20$ K. Light (spectral range 1500–2000 Å) from a modified short-arc high-pressure Xe lamp (EG & G Model FX 193U), which was fitted with a sapphire or CaF_2 window, was focused with an $f = 4$ CaF_2 lens onto the jet parallel to the nozzle slit at a distance $x = 8$ mm. The light beam was split by a CaF_2 plate and monitored by two photomultipliers coated with a (tetraphenyl butadiene) convector, both before and after crossing the planar jet. The absorption $\Delta I/I_0$ was normalized to the incident light intensity.

VUV absorption spectra of jet-cooled aromatic molecules provided information on intramolecular dynamics of odd-parity Rydberg states and an interference between Rydberg and intravalence excitations. The electronic origin of the $3P_{x,y}(^1A_{2u})$ Rydberg excitation [$3P_{x,y}(0)$] of benzene and of benzene-D_6 (Fig. 1) is superimposed on the $^1A_{1g} \rightarrow {}^1E_{1u}$ intravalence transition.[14,15] The energy of $3P_{x,y}(0)$ (55 877 cm^{-1} for C_6H_6 and 55 946 cm^{-1} for C_6D_6) is in accord with one-[14,15] and three-photon[16] bulb spectroscopy. The line shape of $3P_{x,y}(0)$ is a Lorentzian (Fig. 1) with a width (FWHM) of $\Delta = 32.7 \pm 3.1$ cm^{-1} for C_6H_6 and $\Delta = 29.0 \pm 2.0$ cm^{-1} for C_6D_6. The homogeneous linewidths Γ and lifetimes τ obtained after correction for instrumental resolution are $\Gamma = 28 \pm 3$ cm^{-1} ($\tau = 0.19 \pm 0.02$ ps) for C_6H_6, and $\Gamma = 24 \pm 2$ cm^{-1} ($\tau = 0.22 \pm 0.02$ps) for C_6D_6. Our value $pf\Gamma$ for $3P_{x,y}(0)$ is close to the linewidths of 27–33 cm^{-1} reported[6] for the vibronically induced two-photon transitions of this Rydberg transition. A small ($\sim 10\%$) normal deuterium isotope effect on the relaxation rate may exist, which is, however, within our experimental uncertainty, implying that the electronic relaxation process of $3P_{x,y}(0)$ is characterized by moderate energy gap(s). The homogeneous line broadening of the $^1A_{1g} \rightarrow {}^1E_{1u}$ intravalence excitation of jet-cooled benzene exceeds Γ for $3P_{x,y}(0)$ by about one to two orders of magnitude, which is in accord with old arguments,[17] so that the intramolecular relaxation of the intravalence $^1E_{1u}$ excitation presumably occurs within ~ 10 fs, i.e., on a time scale comparable with a vibrational period. The Lorentzian line shape of $^1A_{1g} \rightarrow 3P_{x,y}(0)$ provides compelling evidence for the absence of Rydberg-intravalence interference effects[15,18,19] in benzene, which is in accord with Rice *et al.*[15] The absence of Fano interference effects[20] can be rationalized within the framework of a random coupling model[21,22] for the $3P_{x,y}(0)$–$^1E_{1u}$ interstate coupling terms and for the $^1A_{1g} \rightarrow {}^1E_{1u}$ transition moments to the homogeneously broadened background manifold, which erode all interference effects.[21,22] Pronounced Rydberg-intravalence interference effects[18] are exhibited in the spectrum of jet-cooled naphthalene (Fig. 2). The excessive line broadening of the resonance, e.g., $\Gamma = 80$ cm^{-1} ($\tau = 70$ fs) for the $R_c^5 + 1360$ transition (Fig. 2), is close to the corresponding

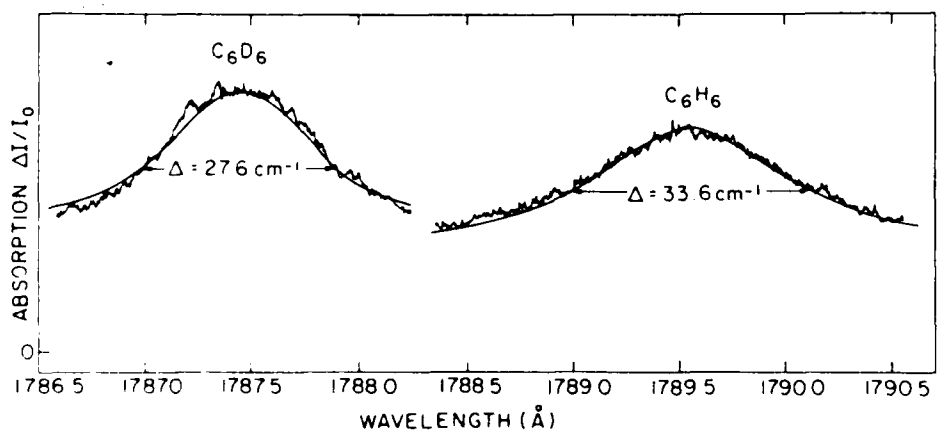

FIG. 1. Absorption spectra of the $^1A_{1g} \rightarrow 3P_{x,y}(^1A_{2u})$ electronic origin of benzene and benzene-D_6 in pulsed planar supersonic expansions of Ar at $p = 105$ Torr. The spectral resolution is 0.45 Å. The base line is marked as zero on the intensity scale. The solid curves represent fits of the line shape $L(\lambda)$ to a Lorentzian superimposed on a constant background $L(\lambda) = A + C/[(\lambda - \lambda_0)^2 + (\Delta/2)^2]$. For C_6H_6: $A = 5.7$, $C = 17.2$ (in arbitrary units), $\lambda_0 = 1789.65$ Å and $\Delta = 1.08$ Å (33.7 cm^{-1}) while for C_6D_6: $A = 6.5$, $C = 12.6$ (in arbitrary units), $\lambda_0 = 1787.45$ Å and $\Delta = 0.88$ Å (27.5 cm^{-1}).

 0021-9606/85/094378-02$02.10 © 1985 American Institute of Physics

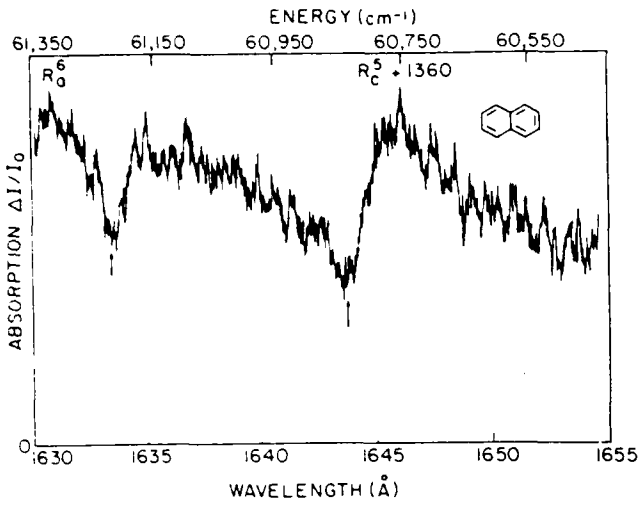

FIG. 2. The absorption spectra of naphthalene in pulsed planar expansions of Ar (p = 105 Torr) in the region 1630–1650 Å. The spectral resolution is 0.5 Å. The antiresonances corresponding to the $R_c^5 + 1360$ and to the R_a^6 Rydberg states (according to the assignment of Refs. 15 and 19) are marked by arrows.

room temperature value $\Gamma = 75\ \text{cm}^{-1}$,[15,19] whereupon the excessive homogeneous broadening make the thermal congestion effects. Our spectroscopic approach can readily be extended throughout the LiF region (up to 11 eV) and will contribute towards the elucidation of the microscopic aspects of intramolecular dynamics and photochemistry.

AA acknowledges the partial support of the work by the Basic Research Fund of the Israel Academy of Sciences, Jerusalem.

[1]D. H. Levy, Annu. Rev. Phys. Chem. **31**, 197 (1980).
[2]A. Amirav, U. Even, and J. Jortner, J. Chem. Phys. **74**, 3745 (1981).
[3]J. A. Syage, W. R. Lambert, P. M. Felker, A. H. Zewail, and R. M. Hochstrasser, Chem. Phys. Lett. **88**, 266 (1982).
[4]B. J. Van der Meer, H. Th. Jonkman, J. Kommandeur, and W. L. Meerts, Chem. Phys. Lett. **92**, 565 (1982).
[5]J. Jortner and S. Leach, J. Chim. Phys. **77**, 7 (1980).
[6]R. L. Whetten, K. J. Fu, and E. R. Grant, J. Chem. Phys. **79**, 2626 (1983).
[7]S. R. Grubb, R. L. Whetten, A. C. Albrecht, and E. R. Grant, Chem. Phys. Lett. **108**, 420 (1984).
[8]S. G. Grubb, C. E. Ottis, R. L. Whetten, E. R. Grant, and A. S. Albrecht, J. Chem. Phys. **82**, 1135 (1985).
[9]R. L. Whetten, K. J. Fu, and E. R. Grant, Chem. Phys. **90**, 155 (1984).
[10]J. M. Wiesenfeld and B. I. Greene, Phys. Rev. Lett. **51**, 1745 (1983).
[11]A. Amirav and J. Jortner, Journal **94**, 545 (1983).
[12]A. Amirav and J. Jortner, Journal **95**, 295 (1983).
[13]A. Amirav, M. Sonnenschein, and J. Jortner, Chem. Phys. Lett. **100**, 488 (1983).
[14]P. G. Wilkinson, Can. J. Phys. **34**, 596 (1956).
[15]R. Scheps, D. Florida, and S. A. Rice, J. Chem. Phys. **56**, 295 (1972).
[16]P. M. Johnson and G. M. Konenowski, Chem. Phys. Lett. **97**, 53 (1983).
[17]J. Jortner, J. Chim. Phys. **1970**, 10.
[18]J. Jortner, and G. C. Morris, J. Chem. Phys. **51**, 3689 (1969).
[19]D. Florida, R. Scheps, and S. A. Rice, Chem. Phys. Lett. **15**, 490 (1972).
[20]U. Fano, Phys. Rev. **124**, 1866 (1961).
[21]M. L. Sage and J. Jortner, Chem. Phys. Lett. **62**, 451 (1979).
[22]S. D. Druger, J. Chem. Phys. **67**, 3238, 3249 (1977).

Volume 115, number 3 CHEMICAL PHYSICS LETTERS 5 April 1985

ENERGY-RESOLVED AND THERMALIZED PHOTOISOMERIZATION RATES OF DIPHENYLBUTADIENE

Jürgen TROE

Institut für Physikalische Chemie der Universität Göttingen, Tammannstrasse 6, D-3400 Gottingen, West Germany

Aviv AMIRAV and Joshua JORTNER

Department of Chemistry, Tel Aviv University, 69978 Tel Aviv, Israel

Received 24 January 1985

Recent measurements of energy-resolved photoisomerization rates of jet-cooled diphenylbutadiene molecules are analyzed in terms of RRKM calculations. Perfect agreement over a wide energy range is obtained. A comparison of the thermally averaged rates with liquid-phase data is made.

1. Introduction

The photoisomerization reactions of trans-stilbene and all-trans-diphenylbutadiene in recent years have been intensively studied under isolated-molecule conditions in low-pressure gases and in supersonic beams, and in the liquid phase. In the gas phase, one of the important aspects was the question whether statistical unimolecular rate theory can quantitatively account for the energy-resolved rates of the non-radiative processes involved. In the liquid phase, basic theories for barrier-overcoming in viscous media, such as Kramers' theory, were tested. In order to conduct a meaningful analysis of the liquid-phase data, a direct comparison with the gas-phase data appears obligatory. In Kramers' theory [1], the low-viscosity limit of a double-well isomerization reaction is given by the conventional "limiting high-pressure rate constant" of a thermal unimolecular reaction

$$k_\infty = \int_{E_0}^{\infty} f(E)\, k(E)\, \mathrm{d}E\,, \qquad (1)$$

with the thermal equilibrium distribution $f(E)$, the threshold energy E_0, and the specific rate constant $k(E)$. Energy-resolved gas-phase experiments give direct assess to $k(E)$. In Kramers' theory, viscosity effects in the liquid produce a decrease of the thermalized rate constants below the maximum value of eq. (1). It is, therefore, an important question whether thermal averaging of the specific rate constants $k(E)$ from isolated-molecule experiments provides an upper limit for the liquid-phase rate constants.

This question was addressed in a previous article by one of us [2] on the photoisomerization of trans-stilbene. By combining the isolated-molecule–energy-resolved photoisomerization results from jet-cooled [3–5] and thermal-distribution [6,7] experiments, it was possible to obtain an optimized RRKM fit which perfectly represented the experimental data of $k(E)$. Calculating k_∞ for this RRKM fit led to the surprising result that liquid-phase data were larger, and not smaller, than "k_∞" by up to one order of magnitude. Possible explanations for this phenomenon are [2], e.g., solvent shifts of the 0–0 transition, the threshold energy E_0, or the activated complex frequencies, which even for small shifts have a large influence in low-barrier unimolecular reactions, or, alternatively, incomplete vibrational relaxation of the lowest vibrational levels in the liquid phase.

Obviously, a similar analysis is of interest for the photoisomerization of diphenylbutadiene. There are recent energy-resolved measurements of $k(E)$ in jet-cooled molecules by Zewail and co-workers [8] over

0 009-2614/85/$ 03.30 © Elsevier Science Publishers B.V. (North-Holland Physics Publishing Division)

the range 0–1800 cm^{-1} and by Amirav et al. [9] over the range 0–7500 cm^{-1}. On the other hand, there are low-viscosity liquid-phase results by Fleming and coworkers [10,11] over a wide temperature range. A preliminary comparison of gas- and liquid-phase data in ref. [12] was conducted only in a qualitative way. In our present work, at first, we try to obtain an optimized RRKM fit of $k(E)$ over the full energy range 0–7500 cm^{-1} of the gas-phase experiments. With these results, we calculate $k_\infty(T)$ and compare with the experiments in liquid ethane by Courtney and Fleming [11], in order to compare with the gas-phase/liquid-phase discrepancies realized in the trans-stilbene system.

2. Specific rate constants $k(E)$

We do our RRKM fit for the gas-phase experiments in the same way as described in ref. [2] for trans-stilbene. We use the complete set of 84 excited-state molecular frequencies calculated by Pierce and Birge [13]. For simplicity, we fit the activated-complex frequencies by multiplying all 37 frequencies related with butadienic carbon atoms (such as indicated in table 2 of ref. [13]) with a common scaling factor F. We use mode 84 (57 cm^{-1}) as being closest to the reaction coordinate. As observed before [2,14], scaling of a set of frequencies or of a single frequency does not result in different fits of $k(E)$. (In trans-stilbene either 15 ethylenic carbon related frequencies or a single frequency out of the 72 molecular oscillators could be scaled [2].) The threshold energy was varied around the apparent threshold of 1050 cm^{-1} which was "visually" observed in ref. [8]. E_0 and the scaling factor F were the only two parameters varied to obtain a fit with the measured $k(E)$ curve. Since there were no internal rotors, the Beyer–Swinehart counting algorithm with an energy graining of 1 cm^{-1} provided an exact count of activated-complex number of channels $W(E - E_0)$ and molecular density of states $\rho(E)$ entering into the standard statistical formula

$$k(E) = W(E - E_0)/h\rho(E) . \qquad (2)$$

For this molecule, $W(E - E_0)$ contains a factor of 2 for the symmetry number.

Table 1 and fig. 1 give $k(E)$ calculations for various parameter sets. An optimum agreement is obtained with E_0 = 1100 cm^{-1} and F = 1.11. F values larger

Table 1
RRKM calculations for the photoisomerization of diphenylbutadiene: specific rate constants $k(E)$ and high-pressure rate constants $k_\infty(T)$ (for molecular and activated-complex parameters, see text)

E (cm^{-1})	$k(E)$ (s^{-1})	E (cm^{-1})	$k(E)$ (s^{-1})
1100	5.01×10^7	1600	1.42×10^9
1150	1.10×10^8	2000	3.60×10^9
1200	1.64×10^8	2500	7.06×10^9
1250	2.65×10^8	3000	1.10×10^{10}
1300	3.67×10^8	3500	1.50×10^{10}
1350	5.06×10^8	4000	1.91×10^{10}
1400	6.70×10^8	5000	2.71×10^{10}
1450	8.28×10^8	6000	3.46×10^{10}
1500	1.00×10^9	7000	4.14×10^{10}
1550	1.21×10^9	8000	4.77×10^{10}

k_∞ (260 K) = 3.27×10^9 s^{-1} k_∞ (290 K) = 5.80×10^9 s^{-1}
k_∞ (270 K) = 4.02×10^9 s^{-1} k_∞ (300 K) = 6.83×10^9 s^{-1}
k_∞ (280 K) = 4.86×10^9 s^{-1}

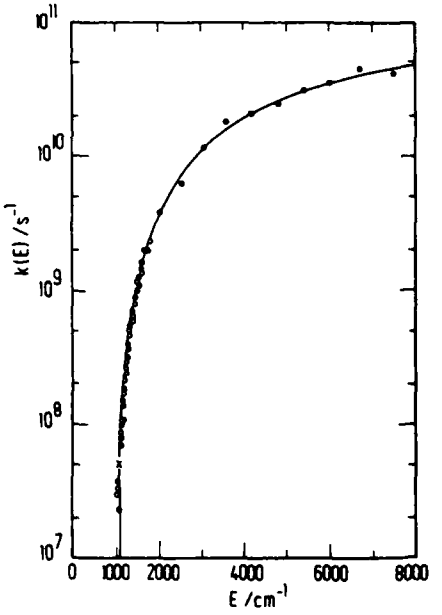

Fig. 1. Specific rate constants $k(E)$ for isomerization of excited diphenylbutadiene (supersonic beam experiments from ref. [8] (o) and ref. [9] (•); optimized RRKM fit from this work (full line, E_0 = 1100 cm^{-1}, F = 1.11), with the calculated threshold rate constant ×).

than unity indicate a "more rigid" set of activated-complex frequencies as compared with the molecular frequencies. A similar extent of rigidity as in the present case was observed in trans-stilbene where $F = 1.2$ was fitted with about half the number of ethylenic carbon related molecular modes [2]. Fig. 1 demonstrates nearly perfect agreement between statistical unimolecular rate theory (here in rigid RRKM form) and experiment. We emphasize again that this remarkable agreement does not necessarily imply complete intramolecular randomization, since, in principle, minor non-random effects could be compensated by the parameter-fitting procedure. Until complete information concerning the potential surfaces of the system becomes available, the RRKM analysis cannot provide a conclusive answer to the cardinal issue of randomization. Nevertheless, the optimized RRKM calculation provides a quantitative fit of the data. Since the fit is done by the variation of two parameters, E_0 and F, an independent fit of E_0 is not possible. However, a value of

$$E_0 = 1100 \pm 50 \text{ cm}^{-1} \quad (3)$$

probably encompasses the widest uncertainties possible.

Whereas the data are perfectly represented over the energy range 1150–7500 cm^{-1}, there is a minor problem at energies below 1150 cm^{-1}. The detailed measurements of quantum yields and non-radiative rates in this range [8,9] indicate a break in the $k(E)$ curve near 1050 cm^{-1} with $k_{nr}(E) \neq 0$ below $E_0 = 1100$ cm^{-1}. At present it is difficult to provide an unambiguous interpretation of the low-energy tail of the $k_{nr}(E)$ curve. The marked break at 1050 cm^{-1} indicates the presence of an additional, slow parallel non-radiative channel, e.g., intersystem crossing, competing with the isomerization. On the other hand, there might be rotational effects in the $k(E,J)$ curve near the threshold energy. Such effects have been explicitly demonstrated, even for a rigid RRKM case, in the dissociation $H_2CO \rightarrow H_2 + CO$ [15]. The effects are most pronounced for small J near the threshold energy. Since the residual J-distribution in the supersonic beam experiments is not exactly known, it is difficult to provide a quantitative account similar to ref. [15]. However, J-effects and the presence of a second channel, probably an intersystem crossing [10], may account for the minor discrepancies with the $k(E)$ calculation near the threshold energy. For this reason, it appears to be preferred to rely on the threshold energy E_0 derived from a fit of the full $k(E)$ curve as given by eq. (3) rather than on the "visual" threshold energy.

3. Comparison of gas- and liquid-phase data

In previous liquid-phase work, Courtney and Fleming [11] attempted to search for the low-viscosity turnover of the Kramers' theory [1] by measuring the photoisomerization rate in liquid ethane and propane at temperatures between 260 and 297 K. In these experiments the viscosity and the temperature were simultaneously varied so that viscosity effects and changes in the Boltzmann factor are hard to disentangle. Measurements with varying viscosity for one solvent at constant temperature, such as performed by Brey et al. for stilbene [16] in high-pressure liquids, or by Troe and co-workers [17,18] with halogens in solvents with densities varying continuously from the low-pressure gas phase to high-pressure liquid conditions, are not available for diphenylbutadiene. Therefore, an unambiguous analysis of the liquid-phase data alone appears impossible.

Our present calculation of specific rate constants $k(E)$ permits us to construct the corresponding high-pressure rate constants k_∞ via eq. (1). Table 1 includes $k_\infty(T)$ values for our optimized RRKM model. A comparison with the experimental data of Courtney and Fleming [11] in liquid ethane is made in fig. 2.

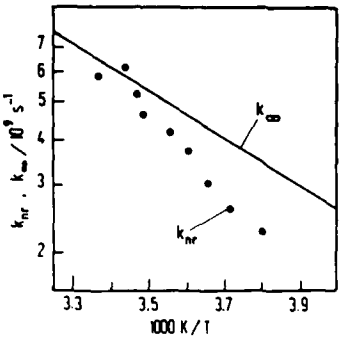

Fig. 2. Comparison of "high-pressure rate constant" k_∞ (this work) with measurements of thermalized photoisomerization rate constants k_{nr} for diphenylbutadiene in liquid ethane (experimental points • from ref. [11]).

Quite unlike trans-stilbene, where the non-radiative rate constant, k_{nr}, in liquid solvents was found to be markedly larger than k_∞ (up to one order of magnitude), for diphenylbutadiene k_{nr}, in liquid C_2H_6, is slightly below k_∞. It also shows a markedly different temperature coefficient. Whereas k_∞ is represented (between 260 and 300 K) by

$$k_\infty = 8.3 \times 10^{11} \exp(-1000\ \mathrm{cm}^{-1}\ hc/kT)\ \mathrm{s}^{-1}\ . \quad (4)$$

k_{nr} in liquid ethane (between 263 and 291 K) was found [11] to be equal to

$$k_{nr} = 5.8 \times 10^{13} \exp(-1854\ \mathrm{cm}^{-1}\ hc/kT)\ \mathrm{s}^{-1}\ . \quad (5)$$

The marked differences in apparent activation energies suggest that k_{nr} for liquid ethane is still in a range of marked viscosity effects far below the low-viscosity maximum. It seems to us that the low-viscosity maximum of k_{nr} is higher than k_∞ also in diphenylbutadiene indicating solvent shifts in the molecular parameters of excited diphenylbutadiene. Only experiments in the gas phase can further elucidate this point. Ethane is a particularly suitable solvent for such studies, since density can conveniently be changed in a continuous manner from the low-pressure gas to liquid conditions [17]. Such experiments are underway [19].

4. Conclusions

We have shown that an optimized RRKM fit provides an excellent representation of energy-resolved photoisomerization rates of excited diphenylbutadiene in jet-cooled free molecules. Thermal averaging of the specific rate constants $k(E)$ leads to the high-pressure limiting rate constants k_∞. A comparison of k_∞ with liquid-phase data shows markedly different activation energies. There are strong indications that, as in trans-stilbene, solvent shifts of excited-state molecular parameters occur. Before an analysis of liquid-phase results in terms, for example, of Kramers' theory can be made, these solvent shifts have to be determined. Measurements in one solvent over large density ranges, from low-pressure gases up to high-pressure liquids, have to be conducted before a more meaningful analysis of liquid-phase data appears possible.

Acknowledgement

Discussions of this work with J. Schroeder and financial support from the Deutsche Forschungsgemeinschaft (Sonderforschungsbereich 93 "Photochemie mit Lasern") and from the U.S. Army through its European Research Office is gratefully acknowledged.

References

[1] H.A. Kramers, Physica 7 (1940) 284; S. Chandrasekhar, Rev. Mod. Phys. 15 (1943) 1.
[2] J. Troe, Chem. Phys. Letters 114 (1985) 241.
[3] J. Syage, W. Lambert, P. Felker, A.H. Zewail and R.M. Hochstrasser, Chem. Phys. Letters 88 (1982) 266.
[4] A. Amirav and J. Jortner, Chem. Phys. Letters 95 (1983) 295.
[5] T.J. Majors, U. Even and J. Jortner, J. Chem. Phys. 81 (1984) 2330.
[6] B.I. Greene, R.M. Hochstrasser and R.B. Weisman, Chem. Phys. 48 (1980) 289; J. Chem. Phys. 71 (1979) 544.
[7] J.W. Perry, N.F. Scherer and A.H. Zewail, Chem. Phys. Letters 103 (1983) 1.
[8] J.F. Shepanski, B.W. Keelan and A.H. Zewail, Chem. Phys. Letters 103 (1983) 9.
[9] A. Amirav, M. Sonneschein and J. Jortner, Photoisomerization of Diphenylbutadiene in Supersonic Jets, to be submitted for publication.
[10] S.P. Velsko and G.R. Fleming, J. Chem. Phys. 76 (1982) 3553.
[11] S.H. Courtney and G.R. Fleming, Chem. Phys. Letters 103 (1984) 443.
[12] S.H. Courtney, G.R. Fleming, L.R. Khundkar and A.H. Zewail, J. Chem. Phys. 80 (1984) 4559.
[13] B.M. Pierce and R.R. Birge, J. Phys. Chem. 86 (1982) 2651.
[14] D.C. Astholz, J. Troe and W. Wieters, J. Chem. Phys. 70 (1979) 5107.
[15] J. Troe, J. Phys. Chem. 88 (1984) 4375.
[16] L.A. Brey, G.B. Schuster and H.G. Drickamer, J. Am. Chem. Soc. 101 (1979) 129; J. Chem. Phys. 71 (1979) 2765.
[17] B. Otto, J. Schroeder and J. Troe, J. Chem. Phys. 81 (1984) 202.
[18] H. Hippler, V. Schubert and J. Troe, J. Chem. Phys. 81 (1984) 3931.
[19] J. Schroeder, J. Troe and F. Voss, to be published.

Electron Localization in Alkali-Halide Clusters

Uzi Landman
School of Physics, Georgia Institute of Technology, Atlanta, Georgia 30332, and Institute of Theoretical Physics, Chalmers University of Technology, 412 96 Goteborg, Sweden

and

Dafna Scharf and Joshua Jortner
Department of Chemistry, Tel Aviv University, 69978 Tel Aviv, Israel

(Received 14 January 1985)

The quantum path-integral molecular-dynamics method was applied to explore the structure, energetics, and dynamics of an excess electron interacting with an alkali-halide cluster. Four distinct modes of electron localization were established, which depend on the cluster composition, size, and structure; they involve an internal *F*-center defect, an external surface state, dissociative detachment of an alkali atom, and structural isomerization induced by electron attachment.

PACS numbers: 71.45.Nt, 36.40.+d, 61.20.Ja

Structural, electronic, dynamic, and chemical characteristics of materials depend primarily on the state (phase) and the degree (size) of aggregation. Small clusters, i.e., finite aggregates containing 3–500 particles, exhibit unique physical and chemical phenomena, which are of both fundamental and technological significance, and provide ways and means to explore the "transition" from molecular to condensed-matter systems.[1] Theoretical studies of clusters were hampered by the relatively large number of particles, which renders the adaptation of molecular science techniques rather cumbersome, while the lack of translational symmetry inhibits the employment of solid-state methodology. Molecular-dynamics (MD) simulations, consisting of the generation of phase-space trajectories via the numerical integration of the (classical) equations of motion for a many-particle system, are particularly suitable for the study of the structure and dynamics of small clusters.[2,3] In this context, localized excess electron states in clusters[4] are of considerable interest with regard to the (nonreactive and reactive) mechanisms of electron attachment, the formation of bulk or surface states, and the role of the excess electron as a probe for the interrogation of the nuclear dynamics of the cluster. Futhermore, quantum phenomena are expected to be pronounced in such systems since the electron wavelength is comparable to the cluster size. In this paper we report on the structure, energetics, and dynamics of alkali-halide clusters (AHC) studied with classical MD, and of electron alkali clusters studied with the quantum path-integral MD method (QUPID).[5-8] AHC were chosen since the nature of the interionic interactions is well understood and in view of the abundance of model calculations and experimental information of these systems.[9] Our QUPID calculations establish four modes of localization of an excess electron in AHC: (i) an *F*-center defect with the excess electron replacing an internal halide ion; (ii) a new surface state, i.e., a "surface *F* center" of the excess electron; (iii) dissociative electron attachment to AHC resulting in the formation of an "isolated" alkali atom; (iv) structural isomerization induced by electron attachment. Our calculations establish the compositional, structural, and size dependence of these various localization mechanisms.

The QUPID method[6-8] was applied to a system of an electron interacting with an AHC consisting of N ions (N_1 cations and N_2 anions). The interionic potential energy within the AHC is $V_{\mathrm{AHC}}=\sum_{i<j}\Phi_{ij}(R_{ij})$, with the interionic pair potentials $\Phi_{ij}(R_{ij})$ being given by the Born-Mayer potential with the parameters determined by Fumi and Tosi.[10] The electron-AHC potential is $V_e(\mathbf{r})=\sum_l\Phi_{el}(\mathbf{r}-\mathbf{R}_l)$ consisting of a sum of electron-ion potentials, which are described by the purely repulsive pseudopotential $\Phi_{el}(r)=e^2/r$ for the electron-anion interaction and by the local pseudopotential[11] $\Phi_{el}(r)=-e^2/R_c$, $r\le R_c$, and $\Phi_{el}(r)=-e^2/r$, $r>R_c$, for the electron–positive-ion interaction. The Hamiltonian is $H=K_e+V_e+K_{\mathrm{AHC}}+V_{\mathrm{AHC}}$, where K_e and K_{AHC} are the kinetic-energy operators for the electron (mass m) and of the ions (masses $M_l=M_1$ and M_2), respectively. Observables are obtained from the quantum partition function $Z=\lim_{p\to\infty}[Z_p]^p$ with

$$Z_p=\mathrm{Tr}[\exp(-\tau K_{\mathrm{AHC}})\exp(-\tau K_e)\exp(-\tau V_{\mathrm{AHC}})\exp(-\tau V_e)],$$

where $\tau=\beta/p$ and $\beta=(k_BT)^{-1}$ is the inverse temperature. If we make use of the free particle propagator[12] Z_p is

$$Z_p=\prod_{\alpha=1,2}\left(\frac{M_\alpha}{2\pi\tau\hbar^2}\right)^{3N_\alpha p/2}\left(\frac{m}{2\pi\tau\hbar^2}\right)^{3p/2}\int\prod_{l=1}^{N}d^3R_l\prod_{i=1}^{p}d^3r_i\exp[-\beta(V_{\mathrm{eff}}^e+V_{\mathrm{eff}}^l)], \quad (1)$$

© 1985 The American Physical Society

where

$$V_{\text{eff}} = \sum_{i=1}^{p} \left[\frac{pm}{2\hbar^2\beta^2} (\mathbf{r}_i - \mathbf{r}_{i+1})^2 + V_e(\mathbf{r}_i)/p \right]$$

and

$$V'_{\text{eff}} = \sum_{I=1}^{N} \sum_{i=1}^{p} \frac{pM_I}{2\hbar^2\beta^2} (\mathbf{R}_{I(i)} - \mathbf{R}_{I(i+1)})^2 + V_{\text{AHC}}/p.$$

Equation (1) maps the quantum problem onto the classical statistical mechanics of $N+1$ particles, each consisting of a periodic chain (necklace) of p pseudoparticles (beads) with nearest-neighbor harmonic interchain interactions, whose strengths depend upon the masses (m, M_1, M_2), the temperature (T), and the pseudoparticle number (p). When the thermal wavelength [$\lambda_T = (\beta\hbar^2/M_I)^{1/2}$] is smaller than any relevant length scale, the Gaussian factor in Z_p reduces to a delta function and the necklace collapses to a classical particle. This is the case for the ionic part of our system. The average energy of the system is given at equilibrium by

$$E = \frac{3N}{2\beta} + \langle V_{\text{AHC}} \rangle + K_e + p^{-1} \left\langle \sum_{i=1}^{p} V_e(\mathbf{r}_i) \right\rangle$$

with the electron kinetic energy

$$K_e = \frac{3}{2\beta} + \frac{1}{2p} \sum_{i=1}^{p} \left\langle \frac{\partial V_e(\mathbf{r}_i)}{\partial \mathbf{r}_i} \cdot (\mathbf{r}_i - \mathbf{r}_p) \right\rangle$$

which consists of the free-particle term ($3/2\beta$) and the contribution from the interaction (K_{int}) with the ions.[13] The statistical averages indicated by angular brackets are over the Boltzmann distributions as defined in Eq. (1). This formalism is converted into a numerical algorithm by noting[14] the equivalence of the sampling described above to that over phase-space trajectories generated via MD by the classical Hamiltonian

$$H = \sum_{i=1}^{p} \frac{m^* \dot{\mathbf{r}}_i^2}{2} + \sum_{I=1}^{N} \frac{M_I \dot{\mathbf{R}}_I^2}{2} + \sum_{i=1}^{p} \left[\frac{pm(\mathbf{r}_i - \mathbf{r}_{i+1})^2}{2\hbar^2\beta^2} + \frac{V_e(\mathbf{r}_i)}{p} \right] + V_{\text{AHC}}, \tag{2}$$

the mass m^* being arbitrary and taken as $m^* = 1$ u.

Numerical simulations were performed for an electron interacting with sodium-chloride clusters at about room temperature. On the basis of examination of the stability of the variance of the kinetic-energy contribution K_{int}, the number of "electron beads" was taken as $p = 399$. By use of an integration step of $\Delta t = 1.03 \times 10^{-15}$ sec, long equilibration runs were performed [$(1\text{–}2) \times 10^4 \Delta t$]. The reported results were obtained via averaging over $8 \times 10^3 \Delta t$, following equilibration. The electron-ion pseudopotential parameters were varied by changing the cutoff radius R_c in the range $(3.22\text{–}5.29)a_0$. From QUPID calculations on a single Na atom, the atomic ionization potential is reproduced (see Table I) for $R_c = 5.29a_0$, which seems to be a too-high value for the characterization of this pseudopotential.[6] Therefore, on the basis of pseudopotential parametrization studies[11] and a recent QUPID study[8] of F centers in molten and solid KCl in which the same form of pseudopotential was employed, a value of $R_c = 3.22a_0$ (yielding a value of -0.3005 a.u. for the electron binding energy to Na^+, see Table I) is preferred. Fortunately, our conclusions regarding internal and surface-localization modes remain unchanged with respect to reasonable variations of this parameter. In simulations involving the electron-AHC interaction, different initial conditions were employed, two of which for the $[Na_{14}Cl_{13}]^+$ system are portrayed in Figs. 1(a) and 1(b). The resulting final state of the system was found to be independent of the initial conditions.

It has previously been suggested on the basis of zero-temperature structural calculations,[9] and has been confirmed by our classical MD simulations, that when the size of the clusters increases ($N \geq 20$), the NaCl cyrstallographic arrangement is preferred for particular stability for clusters forming rectangular structures even if the number of positive and negative ions is not equal. Therefore, we have chosen to study first the interaction of an electron with $[Na_{14}Cl_{13}]^+$ and $[Na_{14}Cl_{12}]^{++}$ clusters, which exhibit pronounced stability. In Figs. 1(c) and 1(e), we present our results (using $R_c = 3.22a_0$) for the equilibrium electron-charge distribution obtained from 2D projections of the necklace edge points, and for the nuclear configuration of the clusters. In both cases the electron, which starts in either initial configuration as shown in Figs. 1(a), 1(b), has been localized. However, two distinct modes of electron localizations are exhibited involving *internal* and *external localization* for the doubly charged and singly charged cluster, respectively. The vacancy-containing configuration of the $[Na_{14}Cl_{12}]^{++}$ cluster stabilizes an internally localized excess electron state, with the e surrounded by six Na^+ ions in an octahedral configuration and by twelve Cl^- ions [Fig. 1(e)] which is similar to the case of an F center in the extended solid. The electron affinity of the cluster $E_A = E_B^g + E_c$ is obtained by summing the electron binding energy

$$E_B^g = \frac{3}{2\beta} + K_{\text{int}} + p^{-1} \sum_{i=1}^{p} \langle V_e(\mathbf{r}_i) \rangle$$

and the cluster reorganization energy $E_c = \langle V_{\text{AHC}} \rangle - \langle V_{\text{AHC}} \rangle_0$, where $\langle V_{\text{AHC}} \rangle_0$ is the potential energy of the "bare" AHC in the absence of the electron. The ionic configuration of the e-$[Na_{14}Cl_{12}]^{++}$ cluster is somewhat distorted; however, the gain in E_B^g (-0.249

TABLE I. Average equilibrium temperature ($\langle T \rangle$), interionic cluster potential energy ($\langle V_{AHC} \rangle$), electron interaction kinetic energy (K_{int}), electron kinetic energy $K_e = 3/2\beta + K_{int}$, e-AHC interaction potential energy ($\langle V_e \rangle$), electron binding energy (E_B^e), cluster reorganization energy (E_c), electron affinity of cluster (E_A), and Cartesian components of the "electron necklace" gyration radii (R_x^2, R_y^2, R_z^2). Atomic units are used (energy and $\langle T \rangle$ in Hartrees, length in Bohr radii). Variances are given in parentheses. Calculated values of $\langle T \rangle$ and $\langle V_{AHC} \rangle$ for the "bare" clusters: $[Na_{14}Cl_{14}]$, $0.976(0.111) \times 10^{-3}$, -3.7296; $[Na_{14}Cl_{13}]^+$, $0.948(0.106) \times 10^{-3}$, -3.5911; $[Na_{14}Cl_{12}]^{++}$, $0.954(0.093) \times 10^{-3}$, -3.3151; $[Na_5Cl_4]^+$, $1.01(0.38) \times 10^{-3}$, -1.0999.

	$10^3\langle T \rangle$	$\langle V_{AHC} \rangle$	$10^2 K_{int}$	K_e	$\langle V_e \rangle$	E_B^e	E_c	E_A	R_x^2	R_y^2	R_z^2
e-$[Na_{14}Cl_{13}]^+$	0.983	−3.4856	6.4195	0.0657	−0.2251	−0.1594	0.1055	−0.0539	5.4	7.0	9.8
$R_c = 3.22$	(0.035)		(0.633)								
e-$[Na_{14}Cl_{13}]^+$	0.972	−3.5768	1.5182	0.0166	−0.0700	−0.0534	0.0143	−0.0391	23.5	23.2	55.2
$R_c = 5.29$	(0.031)		(0.426)								
e-$[Na_{14}Cl_{12}]^{++}$	0.938	−3.2372	7.2203	0.0736	−0.3226	−0.2490	0.0799	−0.1691	4.6	6.8	6.3
$R_c = 3.22$	(0.028)		(0.767)								
e-$[Na_{14}Cl_{12}]^{++}$	0.948	−3.3143	1.9995	0.0214	−0.1365	−0.1151	0.0008	−0.1143	55.3	57.9	43.3
$R_c = 5.29$	(0.025)		(0.956)								
e-$[Na_5Cl_4]^+$	0.950	−1.0059	2.6389	0.0278	−0.3012	−0.2734	0.0940	−0.1794	2.2	2.0	2.5
$R_c = 3.22$	(0.132)		(0.582)								
e-$[Na_5Cl_4]^+$	0.946	−1.0483	3.5453	0.0369	−0.1876	−0.1508	0.0516	−0.0992	5.7	7.2	5.5
$R_c = 4.36$	(0.038)		(0.601)								
e-Na^+	1.038		0.713	0.0087	−0.3092	−0.3005				$R^2 = 3.6$	
$R_c = 3.22$	(0.442)		(0.638)								
e-Na^+	1.043		0.034	0.001 98	−0.2299	−0.2280				$R^2 = 3.4$	
$R_c = 4.36$	(0.527)		(0.049)								
e-Na^+	1.084		0.012	0.0017	−0.18897	−0.1872				$R^2 = 4.9$	
$R_c = 5.29$	(0.574)		(0.032)								

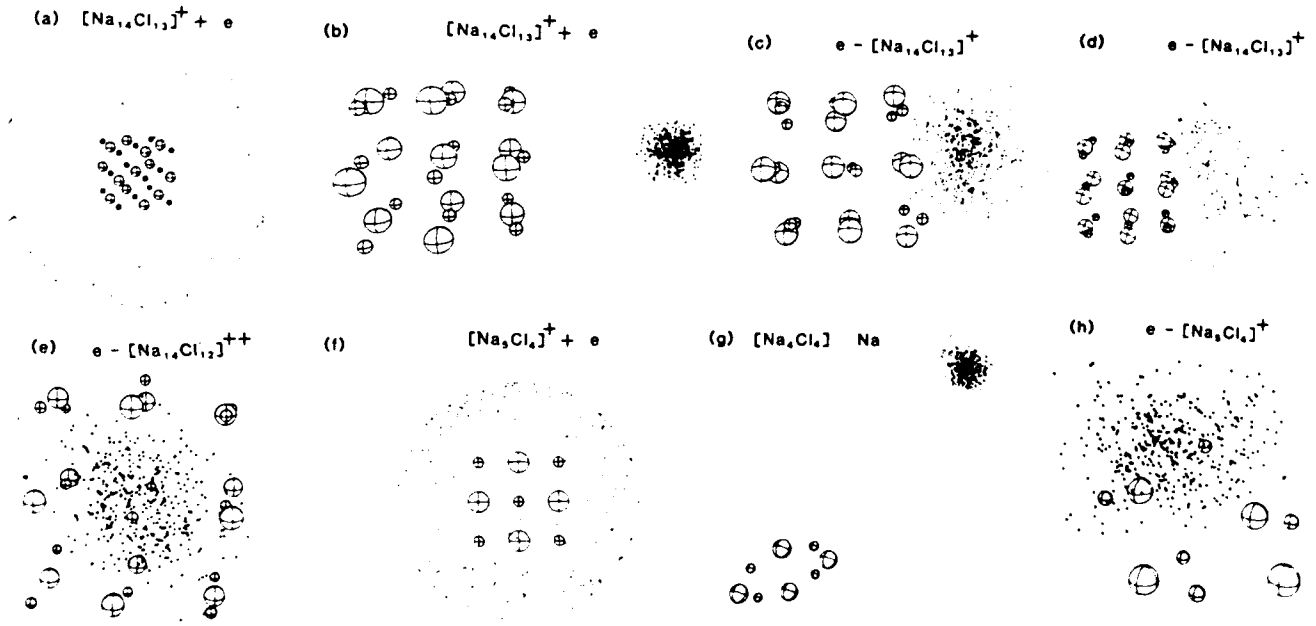

FIG. 1. Ionic configurations and "electron necklace" distributions for an excess electron interacting with sodium-chloride clusters. Small and large spheres correspond to Na^+ and Cl^- ions, respectively. Dots represent 2D projections of the "electron beads." (a),(b) Alternate initial configurations of $[Na_{14}Cl_{13}]^+ + e$ [in (b) the e bead is localized to the right of the cluster] which achieve the equilibrium configurations corresponding to surface states given in (c), $R_c = 3.22a_0$, and (d) $R_c = 5.29a_0$. (e) Equilibrium configuration of e-$[Na_{14}Cl_{12}]^{++}$, $R_c = 3.22a_0$, exhibiting an internal F center. (f) Initial state of e-$[Na_5Cl_4]^+$. (g) Equilibrium configuration of e-$[Na_5Cl_4]^+$ with $R_c = 3.22a_0$ resulting in dissociation of Na. (h) Equilibrium configuration of e-$[Na_5Cl_4]^+$ with $R_c = 4.36a_0$ which corresponds to structural isomerization.

a.u.) exceeds the loss in E_c (0.0799 a.u.) favoring internal localization (Table I). It is of interest to note that the total energy of e-$[Na_{14}Cl_{12}]^{++}$ is rather close to that of $[Na_{14}Cl_{13}]^{+}$, so that the electron binding energy in the cluster is similar to that of a negative ion, analogously to the situation for F-center formation in (extended) ionic crystals,[8] thus establishing the dominance of short-range attractive interactions in electron trapping (localization) phenomena. A drastically different localization mode is obtained in the e-$[Na_{14}Cl_{13}]^{+}$ system [Fig. 1(c)], where a surface state is exhibited. For $R_c = 3.22a_0$ the electron localizes around an Na^+ surface ion [Fig. 1(c)], leaving an essentially neutral $[Na_{13}Cl_{13}]$ cluster, which interacts with the (partially) neutralized Na atom mainly via polarization of the electron cloud (with a residual ionic binding of -0.002 a.u.). We refer to this state as a cluster-surface localized state, which bears close analogy with Tamm's crystal-surface states.[15] When the pseudopotential cutoff R_c increases, the surface state becomes more extended [see Fig. 1(d) for $R_c = 5.29a_0$] [the choice of an abnormally high value for R_c (i.e., $5.29a_0$) prevents internal localization in the $[Na_{14}Cl_{12}]^{++}$ cluster since the internal region is then predominantly repulsive (see Table I), resulting in a surface state]. A measure of the spatial extent of the localized electron is given by the gyration radius of the "electron necklace" $R^2 = (1/2p^2)\langle \sum_{i,j} (\mathbf{r}_i - \mathbf{r}_j)^2 \rangle$, which demonstrates (Table I) the enhanced localization in the e-$[Na_{14}Cl_{12}]^{++}$ system and the anisotropy of the electron distribution in the e-$[Na_{14}Cl_{13}]^{+}$ system. An estimation of the extent of the electron thermal wave packet is obtained also by

$$R_T = \left[\frac{p}{p-1} \sum_{i=1}^{p} \langle (\mathbf{r}_i - \mathbf{r}_{i+1})^2 \rangle \right]^{1/2}$$

which for a free electron at room temperature yields $R_T = \sqrt{3}\lambda_T \simeq 56a_0$ ($\lambda_T \simeq 32.34a_0$). In all the calculations reported herein R_T values of $52a_0$–$55a_0$ were obtained, i.e., the same as the free-electron value to within statistical significance (compare to typical interionic distance of $5a_0$ in NaCl clusters).

In smaller clusters novel effects of dissociative electron attachment and cluster isomerization induced by electron localization will be manifested. We have studied the smallest singly ionized cluster exhibiting high stability, i.e., $[Na_5Cl_4]^+$, for which the lowest energy configuration is planar with four Na^+ ions at the corners and one at the center of an approximate square.[9] This cluster possesses an isomeric structure (less stable by 0.014 a.u.) in which the ions are arranged in a distorted pyramidal configuration.[9] Adding an electron to the ground-state planar configuration of $[Na_5Cl_4]^+$ (with the Na^+ pseudopotential being characterized by $R_c = 3.22a_0$) transforms the system into a neutral $[Na_4Cl_4]$ cluster with a planar ring structure and a dissociated neutral Na atom [Table I and Figs. 1(f) and 1(g), corresponding to the initial- and final-state configurations, respectively]. To demonstrate that this process is driven by the localization of e around a single Na^+ ion, we have performed further simulations by decreasing the cation-electron binding strength, taking $R_c = 4.36a_0$. In this case, extreme localization is not sufficiently counterbalanced by e binding. Instead, the planar structure transforms to the isomeric pyramidal configuration with the electron localized as a diffuse cloud about the tip of the pyramid [Fig. 1(h)]. Electron localization accompanied by structural isomerization will constitute a prevalent phenomenon for AHC with smaller e-cation binding energy, i.e., the heavier alkali metals. In view of the intimate interrelationship between structural isomerization and melting of clusters,[16] it will be interesting to explore the melting of such finite systems induced by electron localization.

This work is supported by the U.S. Department of Energy under Contract No. EG-S-05-5489, and by the U.S. Army through its European Research Office.

[1]See papers in Ber. Bunsenges. Phys. Chem. **88** (1984).
[2]C. L. Briant and J. J. Burton, J. Chem. Phys. **63**, 2045 (1975).
[3]See review by F. F. Abraham, J. Vac. Sci. Technol. **82**, 534 (1984).
[4]J. Jortner, in Ref. 1, p. 188.
[5]D. Chandler and P. G. Wolynes, J. Chem. Phys. **79**, 4078 (1981).
[6]B. De Raedt, H. Sprik, and H. L. Klein, J. Chem. Phys. **80**, 5719 (1984).
[7]D. Chandler, J. Phys. Chem. **88**, 3400 (1984).
[8]M. Parrinello and A. Rahman, J. Chem. Phys. **80**, 860 (1984).
[9]T. P. Martin, Phys. Rep. **95**, 167 (1983).
[10]F. G. Fumi and M. P. Tosi, J. Phys. Chem. Solids **25**, 31, 45 (1964).
[11]R. W. Shaw, Phys. Rev. **174**, 769 (1968).
[12]L. S. Schulman, *Techniques and Applications of Path Integrals* (Wiley, New York, 1981).
[13]M. F. Herman, E. J. Bruskin, and B. J. Berne, J. Chem. Phys. **76**, 5150 (1982).
[14]D. Callaway and A. Rahman, Phys. Rev. Lett. **49**, 613 (1982).
[15]N. F. Mott and R. W. Gurney, *Electronic Processes in Ionic Crystals* (Oxford Univ. Press, Oxford, 1946).
[16]G. Natanson, F. Amar, and R. S. Berry, J. Chem. Phys. **78**, 399 (1983).

END

DATE

FILMED

6-88

DTIC